Доклади на Българската академия на науките
Comptes rendus de l'Académie bulgare des Sciences
Tome 77, No 10, 2024

GEOLOGY
Mineralogy

INCOMPATIBLE ELEMENTS (REE, Th, U, Nb, Ta, Ti) MINERAL ASSOCIATION IN ALTERED PEGMATITE FROM THE DJURKOVO Pb-Zn DEPOSIT, CENTRAL RHODOPES: OCCURRENCE AND GEOCHEMICAL PROPERTIES

Sylvina Georgieva[1]✉, Rossitsa D. Vassileva[1], Valentin Grozdev[1], Georgi Milenkov[1], Jan Cempírek[2], Radek Škoda[2], Elitsa Stefanova[1]

Received on July 23, 2024
Presented by K. Stoykova, Corresponding Member of BAS, on September 17, 2024

Abstract

The Djurkovo base-metal vein deposit in Laki ore field, is hosted by a heterogeneous gneiss/amphibolite/marble rock sequence of the high-grade metamorphic complex of the Central Rhodopes. Mineralogical and geochemical investigation was conducted on slightly deformed, and hydrothermally altered thin pegmatite dykes intruded in the marbles. The pegmatite bodies consist mostly of K-feldspar, albite and quartz, with minor garnet present. Clear textural zonation within the bodies is absent except for the preferential crystallization of garnet in the innermost parts. The main pegmatite accessories include ishikawaite, zircon, apatite, monazite-(Ce), allanite-(Ce), and titanite. The post-magmatic hydrothermal overprint on the pegmatites resulted in the formation of the assemblage including epidote, sericite, chlorite, carbonate, quartz, hematite, and leucoxene. The accessory oxide, silicate, and phosphate minerals bearing rare earth elements (REE), actinides (ACT), Nb, Ta, and Ti have undergone partial replacement by secondary mineral phases (thortveitite, fergusonite, fersmite, uraninite, thorianite, REE-epidote, xenotime) observed as irregular grains or veinlets along fractures and dissolved zones, either inside or near the primary minerals.

Key words: (REE,U,Th)–(Nb,Ta,Ti) oxide minerals, ishikawaite, fergusonite, fersmite, thortveitite

The study is financially supported by the Bulgarian National Science Fund projects KP-06-N34/4 and ERA-MIN PEGMAT project KP-06-DO02/2.
https://doi.org/10.7546/CRABS.2024.10.07

Introduction. The growing interest in pegmatites as sources of industrial materials like feldspar for ceramics, as well as critical elements including Li, Be, Cs, Nb, Ta, and REE, underlines the need for extensive revision and additional investigation in this deposit type [1]. The essential part of these elements, reputed as incompatible elements (IE), have specific geochemical properties and the ability to complex with F, Cl, etc. Typically concentrated in the upper continental crust through magmatic-hydrothermal processes, these elements get strongly fractionated either during the late stages of magma fractional crystallization, or, in specific cases, during low-degree partial melting [2]. Pegmatites, particularly those belonging to the NYF family [3], are characterized by the presence of IE such as REE, actinides (ACT; e.g., Th, U), and HFSE (Zr, Nb, Ta, Ti).

In the Central Rhodopes (South Bulgaria), abundant pegmatite bodies with various thickness, shape and position, intruded in the metamorphic complex hosting the economic vein and metasomatic base metal ore mineralization in this region exists. The current mining activities in the main deposits like Petrovitsa, Krushev Dol, Djurkovo, and Govedarnika, provide opportunities to investigate the mineralogical and chemical properties of these pegmatites and to assess their potential as sources of critical elements.

Recent studies have highlighted significantly elevated concentrations of IE in the pegmatites from the region. Furthermore, processes of hydrothermal alteration have affected the pegmatites, particularly resulting in transformation of their primary mineral association and redistribution of IE evidenced by the formation of new mineral phases [4–10].

This study contributes an insight into the mineralogical and geochemical data about the primary and secondary IE minerals from pegmatites enclosed in marble from the Djurkovo Pb-Zn deposit.

Geological setting. Numerous hydrothermal Pb-Zn(±Ag) ore deposits and occurrences are accumulated in the extensional phase of the tectonic regime in the Rhodope metamorphic complex [11]. The studied pegmatites are embedded in gneiss/amphibolite/marble sequence hosting the Djurkovo base-metal deposit, Laki ore district. The sulphide mineralization is linked to several predominantly NNE-oriented ore-bearing faults extended towards the Borovitsa caldera to the east. The polymetallic mineralization occurs as subvertical veins, formed by open-space filling in the gneisses or as carbonate replacement bodies in the marbles. Two major vein structures, spreading NNE-SSW and named Eastern Apophysis and West 2, respectively, are the principal economic sources in the deposit [12]. A substantial number of pegmatite bodies with differing dimensions and appearance intersecting the metamorphic sequence are essential component of the country rocks. Most pegmatites are deformed, folded, boudinaged and cut by subsequent faulting. Prograde skarn formation due to fluid/rock interaction in the marbles is prior to the main sulphide deposition. Later Pb-Zn mineralization in the deposit is manifested in three successive stages [12]: 1) quartz-pyrite; 2) poly-

metallic (galena, sphalerite); 3) carbonate stage. The related hydrothermal alteration led to formation of adularia, epidote, chlorite, and later carbonatization in pegmatites [13]. The age of the base metal mineralization in Djurkovo deposit is constrained between 32–30 Ma consistent with the hydrothermal K-feldspar $^{40}Ar/^{39}Ar$ thermochronology conducted in Laki ore district [14].

Materials and methods. The samples used in this study were selected from hydrothermally altered small-volume pegmatites ($\leq$ 20 cm wide) intruded in marbles from Djurkovo Pb-Zn deposit, level 550. To study the mineral relationships in the rock samples and to select representative areas, the prepared thin sections were examined using optical microscopy (Leica DM750P, Geological Institute, BAS), CATHODYNE optical cathodoluminescence system (NewTec Scientific, Geological Institute, BAS), and scanning electron microscopy (JEOL JSM-6010PLUS/LA, University of Mining and Geology). The chemical composition of the minerals was analyzed using a Cameca SX100 electron microprobe (EMP) at the Laboratory of Electron Microscopy and Microanalysis, Department of Geological Sciences, Masaryk University, Brno. Wavelength-dispersive mode with the accelerating voltage of 15 kV, a beam current of 4–20 nA and a beam size 2–6 µm were used. The following standards and X-ray $K\alpha$ and $L\alpha$ lines were used: sanidine (Si, Al, K), albite (Na), olivine (Mg), almandine (Fe), fluorapatite (Ca, P), tephroite (Mn), anatase (Ti), chromite (Cr), columbite (Nb), $ScVO_4$ (V), $SrSO_4$ (Sr), topaz (F), vanadinite (Cl), barite (Ba), $LaPO_4$ (La), $CePO_4$ (Ce), $PrPO_4$ (Pr), $NdPO_4$ (Nd), $SmPO_4$ (Sm), $GdPO_4$ (Gd), ThO_2 (Th), U (U). The minor and trace element signatures of the mineral association were analyzed using the LA-ICP-MS system in the Geological Institute, BAS. This system consisted of a New Wave Research (NWR) 193 nm Excimer laser UP-193FX attached to a Perkin-Elmer ELAN DRC-e quadrupole inductively coupled plasma mass spectrometer operating at 6 Hz and with a spot size of 25–50 µm.

Results and discussion. The studied pegmatite dykes are emplaced predominantly concordant to the foliation of the host metamorphics. Their main minerals include K-feldspar, albite, quartz and minor garnet. A clear zonal distribution of the minerals was not observed, except for garnet, which tends to concentrate in the central parts of the pegmatite bodies. Along the pegmatite contacts, late hydrothermal epidote and chlorite are developed, usually in thin veinlets penetrating inwards the volume of the pegmatites (Fig. 1A, B). The late hydrothermal association is complemented also by calcite and hematite. The quantitatively predominant K-feldspar forms massive cm-sized aggregates. Late albite partly dissolved earlier K-feldspar. Among the main pegmatite accessory minerals garnet, fluorapatite, zircon, monazite-(Ce), ishikawaite, allanite-(Ce), and titanite occur (Fig. 1C–K). The chemical composition of the investigated in this study minerals is listed in Tables 1 and 2. The euhedral garnet ($\leq$ 5 mm) usually contains inclusions of K-feldspar, quartz, and apatite. The crystals are cracked indicating brittle deformation. Microfractures that developed in the gar-

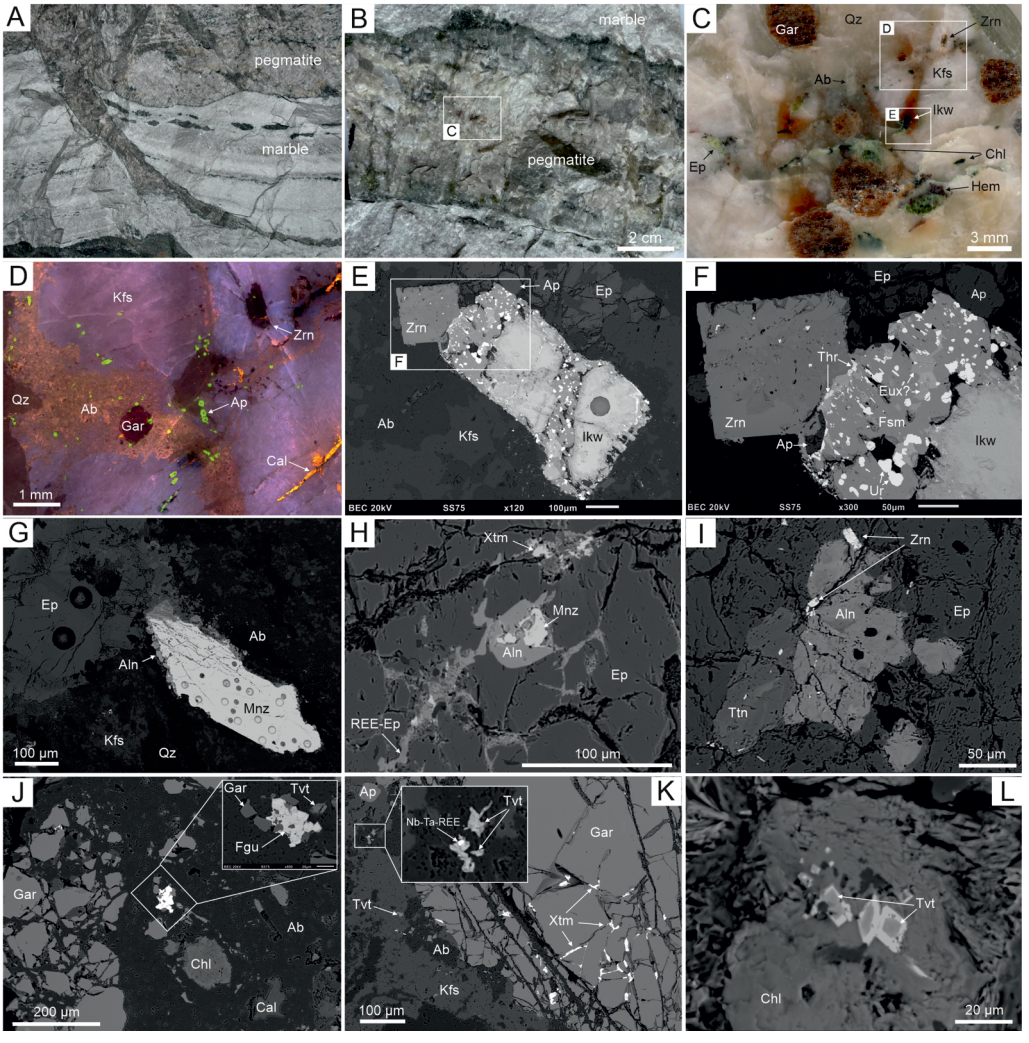


Fig. 1. A, B – macrophotograph of the pegmatite intruded in the marble; C – occurrence and relationships of the primary and secondary hydrothermal mineralization; D – cathodoluminescence (CL) image showing late albitization of the K-feldspar and carbonatization, the clustering of apatite among the mineral boundaries, and the metamictization signs in zircon as radial fractures in the host K-feldspar and absence of luminescence; E–L – BSE images of occurrence and textural relationships between primary accessory minerals and the secondary ones: E–F – different magnification of textural relationships between primary ishikawaite and secondary mineral phases developed on it; G – accessory monazite rimmed by late allanite; H – relics of monazite in allanite, enclosed in epidote with late veinlets of REE-epidote and xenotime; I – allanite, titanite and zircon enclosed in late epidote; J – Late irregular-shaped thortveitite and fergusonite established near garnet; K – anhedral grains of xenotime on cracks in the garnet and late thortveitite with $\leq 5\,\mu m$ inclusion of Nb-Ta-REE phase formed in close proximity to the garnet; L – euhedral zonal thortveitite crystals in chlorite. The zonal pattern is determined by the variation of Y and Sc composition. The brighter rims are rich in Y. Abb.: Kfs – K-feldspar; Qz – quartz; Gar – garnet; Ab – albite; Ep – epidote; REE-Ep – REE-epidote; Chl – chlorite; Cal – calcite; Hem – hematite; Mnz – monazite; Ikw – ishikawaite; Ap – apatite; Aln – allanite; Ttn – titanite; Zrn – zircon; Fsm – fersmite; Eux – euxenite; Xtm – xenotime; Tvt – thortveitite; Fgu – fergusonite; Ur – uraninite; Thr – thorite

Table 1

Representative EPM analyses of the investigated minerals. *The elements in garnet are given in total and are not distributed by positions. V_2O_3, Cr_2O_3, NiO, ZnO, As_2O_5, Rb_2O, SrO, SnO_2, Cs_2O, and BaO were measured but are close to or below detection limits. Mineral abbreviations as in Fig. 1

Mineral	Kfs	Ab	Gar	Fap	Zrn	Mnz-(Ce)	Ikw	Ttn	Aln-(Ce)	Ep	Xtm-(Y)	Tvt	Fgu-(Y)	Fsm	Ur
wt%															
K_2O	15.48	0.12													
Na_2O	1.20	10.96	0.06	0.06											
CaO	0.02	0.57	2.72	55.99		0.29	0.78	24.88	9.21	23.43	0.11	0.17	1.66	16.27	1.39
MgO			0.73				0.05		0.59						
MnO			19.25	0.38			1.42		2.00	0.06	0.63		0.28	0.06	
FeO	0.02	0.24	19.69	0.08	0.03	0.07	8.02		10.52		0.82	0.62	0.75	0.28	
Fe_2O_3									7.24	15.12					
Al_2O_3	17.95	19.26	19.19				0.01	3.38	11.63	21.84		0.77			
SiO_2	64.44	68.12	35.91	0.19	30.30	1.42		31.39	30.61	37.14	3.55	40.95			
P_2O_5				42.27		29.56					29.54		0.06		0.00
TiO_2			0.13		0.01		0.70	34.61	0.64	0.00		0.19	0.22	1.28	
Sc_2O_3			0.16		0.47		1.24				0.40	34.01	0.02	0.12	
Y_2O_3			0.56		0.06	1.92	5.34	4.85	0.47	0.04	40.76	10.60	26.84	1.62	1.22
ZrO_2					58.07		0.39					6.17	0.07	0.27	
Nb_2O_5							44.89	0.54					47.94	73.01	
Ta_2O_5					0.11		2.11						0.92	2.57	
WO_3							0.81						3.92	0.37	
La_2O_3				0.02		12.05	0.00		4.94				0.01	0.05	
Ce_2O_3				0.13	0.02	27.94	0.56		11.59	0.02	0.04		0.06		0.05
Pr_2O_3						3.27	0.20		1.29						0.02
Nd_2O_3				0.15	0.04	11.51	1.30	0.34	4.31		0.19		0.15	0.07	0.01
Sm_2O_3						2.90	1.47		0.68		0.54		0.20	0.03	0.07
Gd_2O_3						2.05	1.87		0.56		1.85	0.45	1.97	0.27	0.20
Tb_2O_3						0.24	0.09				0.63	0.02	0.31	0.06	0.04
Dy_2O_3					0.03	0.75	1.74				6.46	0.90	3.61	0.35	0.34
Ho_2O_3											1.10	0.19	0.51	0.07	
Er_2O_3					0.08	0.16	0.19				3.14	1.20	2.76	0.09	0.11
Tm_2O_3											0.45	0.32	0.47	0.10	
Yb_2O_3					0.12	0.05	0.12				3.62	3.77	3.79	0.18	0.14
Lu_2O_3											0.49	0.64	0.57	0.07	
HfO_2					4.68										
PbO						0.03	0.55				0.28		0.11		0.42
ThO_2					0.09	6.31	4.01		0.87	0.01		0.03		0.73	10.70
UO_2					2.09	0.30	22.55				0.66		2.06	0.71	84.32
F				2.93	0.34										
Cl				0.26											

Table 1

(continued)

apfu															
K	0.920	0.007													
Na	0.109	0.935	0.010	0.009											
Ca	0.001	0.027	0.243	4.829		0.012	0.077	0.876	0.982	2.019	0.004	0.009	0.078	0.961	0.065
Mg			0.090				0.006		0.087						
Mn			1.359	0.026			0.111		0.168	0.004	0.018		0.010	0.003	
Fe^{2+*}	0.001	0.009	1.289	0.006	0.001	0.002	0.618		0.875		0.021	0.022	0.028	0.013	
Fe^{3+}			0.083						0.543	0.916					
Al*	0.986	0.999	1.885				0.001	0.131	1.363	2.070		0.044		0.001	
Si	3.003	2.997	2.993	0.015	0.993	0.055		1.032	3.044	2.988	0.122	1.967			
P				2.881		0.974					0.863				
Ti			0.008				0.049	0.855	0.048			0.007	0.007	0.054	
Sc			0.011		0.013		0.100				0.012	1.423	0.001	0.006	
Y			0.025		0.001	0.040	0.262	0.085	0.025	0.002	0.748	0.271	0.625	0.047	0.029
Zr					0.928		0.018					0.145	0.001	0.007	
Nb							1.874	0.008					0.949	1.843	
Ta					0.001		0.053						0.011	0.005	
W							0.019						0.044	0.039	
La						0.173			0.181					0.001	
Ce				0.004		0.398	0.019		0.422				0.001		0.001
Pr						0.046	0.007		0.047						
Nd				0.004		0.160	0.043	0.004	0.153		0.002		0.002	0.001	
Sm						0.039	0.047		0.023		0.006		0.003		0.001
Gd						0.026	0.057		0.018		0.021	0.007	0.029	0.005	0.003
Tb						0.003	0.003				0.007		0.004	0.001	0.001
Dy						0.009	0.052				0.072	0.014	0.051	0.006	0.005
Ho											0.012	0.003	0.007	0.001	
Er					0.001	0.002	0.005				0.034	0.018	0.038	0.002	0.001
Tm											0.005	0.005	0.006	0.002	
Yb					0.001	0.001	0.003				0.038	0.055	0.051	0.003	0.002
Lu											0.005	0.009	0.008	0.001	
Hf					0.044								0.001		
Pb							0.014				0.003			0.001	0.005
Th					0.001	0.056	0.084		0.020					0.009	0.107
U					0.015	0.003	0.463				0.005		0.020	0.009	0.824
F				0.745											
Cl				0.036											

Table 2

LA-ICP-MS trace-element composition of the investigated minerals. Beryllium, Cr, Co, Ni, Cu, Rb, Mo, Ag, Cd, In, Tl, and Bi were measured but are close to, or below detection limits (bdl). Mineral abbreviations as in Fig. 1

	Gar		Fap		Zrn		Mnz-(Ce)		Ikw		Ttn		Aln-(Ce)		Ep	
	min	max	min	max	min	max	min	max	min	max	min	max	min	max	min	max
P_2O_5, wt%	0.02	0.04	40.84	42.47	0.14	0.43	30.34	30.34	0.01	0.01	0.03	0.10	0.05	0.94	0.01	1.15
Li, ppm	19	55	bdl	3.3	–	–	–	–	0.6	1.1	10	25	bdl	bdl	1.8	47
Sc	445	995	1.2	1.4	2381	4340	bdl	bdl	8126	10 068	26	119	120	379	1.7	53
V	1.3	2.9	0.6	0.6	–	–	–	–	5	5	75	121	49	61	2.3	33
Zn	73	124	bdl	2.8	–	–	–	–	83	124	12	77	127	173	5.5	160
Ga	44	76	10	14	–	–	–	–	56	64	11	36	340	452	59	191
Ge	34	78	17	30	–	–	–	–	170	196	19	43	370	569	6.7	10
As	bdl	bdl	16	24	–	–	–	–	154	198	6.4	39	78	98	8.0	10
Sr	0.1	14	12	110	–	–	–	–	93	197	12	50	104	136	92	286
Y	1299	3393	1654	2055	1987	5427	16 091	27 984	27 887	35 252	3160	6556	2874	4283	4.8	521
Zr	1.0	9.2	bdl	2.7	453 737	519 984	12	12	1525	1552	175	58 062	5.7	545	0.3	73
Nb	0.2	3.2	bdl	0.1	281	599	3.35	3.35	300 000	313 600	2373	4680	3.9	137	0.1	10
Sn	4.4	29	bdl	0.4	–	–	–	–	1356	2170	447	839	42	82	0.7	110
Sb	bdl	bdl	bdl	bdl	–	–	–	–	47	90	1.0	2.6	0.4	0.6	0.5	1.8
Cs	bdl	0.2	bdl	2.3	–	–	–	–	1.1	2.7	0.5	8.5	0.4	6.7	0.2	64
Ba	bdl	0.3	bdl	1.9	–	–	–	–	71	305	2.1	7.9	2.4	3.1	1.0	44
La	0.1	1.3	118	218	0.3	1.0	72 017	143 249	167	178	46	816	16 063	24 606	0.1	411
Ce	0.03	3.7	463	1032	21	44	176 790	327 277	2109	2402	268	2029	32 785	49 669	0.3	904
Pr	0.1	0.8	85	201	0.1	1.2	18 835	34 124	689	794	61	263	3329	4633	0.2	104
Nd	0.8	5.7	505	1025	0.8	10	71 583	126 378	5155	5979	371	1130	12 049	16 817	0.8	350
Sm	6.0	18	253	669	5.1	28	17 801	29 386	6517	8527	220	393	2386	3345	0.6	67
Eu	0.2	0.2	0.9	4.9	0.2	0.5	224	389	17	22	34	78	187	229	0.3	5.7
Gd	42	92	393	625	44	136	12 422	20 473	8532	10 307	311	637	1839	2412	0.4	34
Tb	17	40	65	87	20	55	1306	2287	1773	2086	64	113	179	246	0.2	7.9
Dy	140	409	356	387	183	555	5140	9479	8490	9849	471	806	728	1046	1.4	67
Ho	21	108	40	73	35	119	648	1163	887	972	104	204	100	154	0.3	16
Er	48	453	82	189	106	374	1116	2032	1474	1549	384	797	194	307	0.9	49
Tm	7.0	99	7.9	21	19	67	83	162	166	175	59	143	19	30	0.1	7.1
Yb	47	932	49	111	148	549	317	650	894	985	424	1138	91	163	1.1	41
Lu	4.7	146	5.3	14	18	68	25	57	68	72	60	172	14	24	0.1	5.3
Hf	0.5	1.0	0.36	0.45	27 668	35 384	2.8	9.0	93	119	23	1384	1.1	16	0.1	3.1
Ta	0.1	0.7	bdl	0.1	145	405	0.9	1.2	15 189	21 981	101	249	0.2	0.7	0.1	1.7
W	0.3	0.6	bdl	0.9	–	–	–	–	4299	5142	17	42	1.6	3.0	0.3	1.2
Pb	0.1	2.1	5.2	6.9	2.7	7.6	99	284	1053	1249	3.9	12	39	55	7.1	64
Th	0.1	0.5	4.6	5.4	759	1564	32 872	95 786	23 884	28 429	22	393	4780	9225	0.1	69
U	0.2	2.6	15	19	13 858	19 933	2201	5668	128 336	143 450	209	922	805	1125	0.9	133

net are frequently filled with late xenotime-(Y), whereas thortveitite, fergusonite-(Y), and ≤ 5 µm inclusions of Nb-Ta-REE phases precipitated close to garnet crystal rims, typically among albite and K-feldspar (Fig. 1J–L). The garnet contains high almandine (42.4–49.1 mol.%) and spessartine (39.5–45.3) amounts whereas grossular (2.9–8.2), andradite (0.7–3.6) and pyrope (0.1–3.2) components are low. The LA-ICP-MS shows that the mineral is characterized by incorporation of elevated Y_2O_3 and Sc_2O_3 (< 1 wt.%), low HREE (≤ thousands of ppm), P, Zn, Ga, Ge and Li (≤ hundreds of ppm). Sub- to euhedral, ≤ 200 µm large crystal clusters of fluorapatite are commonly observed among K-feldspar grains, often near the garnet rims or inside garnet volume (Fig. 1D). Its chemical composition reveals high F- and low Cl-content, with incorporation of < 1 wt.% REE_2O_3 and > 1000 ppm Y. Zircon appears as sub- to euhedral mm-sized crystals with µm-sized inclusions of uraninite. The radial fractures in the host K-feldspar and the lack of luminescence in the mineral under cathodoluminescence microscopy indicate that the zircon has undergone metamictization due to high Th and U content (see Fig. 1D). Zircon features elevated contents of HfO_2 (≤ 4.75 wt%), UO_2 (≤ 4.03 wt%), Sc_2O_3 (≤ 0.60 wt%), $HREE_2O_3$ (≤ 0.35 wt%), and thousands of ppm Y and less Th (Fig. 1C–F). Monazite-(Ce) forms ≤ 600 µm sub- to euhedral crystals often rimmed by late allanite-(Ce) and epidote (Fig. 1G). Occasionally, monazite is observed as relic inclusions in lately formed allanite-(Ce) (Fig. 1H). Except for the high amounts of REE_2O_3, monazite-(Ce) is characterized by incorporation of ThO_2 (≤ 9.41 wt.%) and Y_2O_3 (≤ 2.69 wt.%), and thousands of ppm U. Ishikawaite occurs as sub- to euhedral mm-sized crystals commonly replaced in places by the assemblage of fersmite, uraninite and thorite (Fig. 1E–F). An indeterminate phase with a composition similar to U-enriched euxenite with U-content ≤ 30.12 wt% was detected in association with fersmite and uraninite (Fig. 1F). Apart from the high U-content (≤ 24.64 wt.%), the chemical composition of the ishikawaite is characterized by high Y_2O_3 (≤ 5.34 wt.%), Sc_2O_3 (≤ 1.98 wt.%), ThO_2 (≤ 4.90 wt.%) and REE_2O_3 (≤ 7.56 wt.%). Due to metamictization, small amount of SiO_2 is generally measured (≤ 0.14 wt %). Titanite is rarely observed as preserved anhedral ≤ 600 µm grains often in association with allanite-(Ce) and epidote (Fig. 1I) but it is usually replaced by *leucoxene,* quartz and calcite. The chemical composition of the mineral is characterized by incorporation of Y_2O_3 (≤ 4.86 wt.%), Al_2O_3 (≤ 3.61 wt%), Nb_2O_5 (≤ 1.44 wt%), and Nd_2O_3 (≤ 0.34 wt%). Allanite-(Ce) forms anhedral, ≤ 200 µm grains generally enclosed in epidote and in association with titanite and monazite (Fig. 1H, I). Chemically, the mineral contains ≤ 23.37 wt.% REE_2O_3, Y_2O_3 (≤ 1.56 wt%), ThO_2 (≤ 1.00 wt%), MnO (≤ 2.58 wt%), and MgO (≤ 0.74 wt%), ≤ 1125 ppm U, and hundreds of ppm Sc, Ga, Ge, Zn, Sr and Nb. The late epidote mineralization is developed as nests and veinlets in the volume of the pegmatite bodies along with chlorite, hematite and calcite. Epidote formation adjacent to early allanite-(Ce) results in an elevated incorporation of REE and compositions with up to 2069 ppm REE and ≤ 521 ppm Y.

Discussion and conclusions. The studied pegmatite bodies are considered part of the metamorphic host of one of the largest base metal deposits in the Central Rhodopes and hence the whole rock volume is strongly influenced by late hydrothermal events (pre- and syn-ore-forming). The microfractures in the mm-sized accessory minerals (e.g., garnet, monazite, zircon) and the clustering of accessories in polymineralic aggregates are clear indicators of deformation in pegmatites. The latter comprise various accessory minerals concentrating significant amounts of IE (such as REE, Th, U, Nb, Ta, etc.) – part of them assigned as critical for the contemporary industry. The primary accessories (e.g., garnet, ishikawaite, monazite, titanite) affected by late deformation are cracked, altered and replaced by secondary ones (xenotime, thortveitite, fergusonite, fersmite, uraninite, thorite). This deformation, along with later pre- and syn-ore hydrothermal influences, facilitate the extraction of the incompatible chemical elements from primary minerals (e.g., Sc and Y from garnet) and the formation and re-deposition of new μm-sized minerals (e.g., xenotime, thortveitite, fergusonite), either within the volume of the primary accessories along the microfractures, or in close proximity to them. Despite the late hydrothermal activity and metasomatic processes in the Djurkovo Pb-Zn deposit, the limited transport of IE is likely predisposed by environmental constraints, such as the relative concentration and volume of the fluid, pH, ligand activity, and the pressure and temperature as well, in order to influence intense trace element activities. In hydrothermal solutions, chloride and sulphate are the primary ligands responsible for transporting REEs, while fluoride, carbonate, and phosphate are likely significant as depositional ligands, as suggested by Migdisov et al. [15], which is the most expected mechanism for xenotime deposition in the garnet microfractures. The absolute capacity of hydrous fluids to transport incompatible elements and economically significant metals is greatly enhanced by higher pressure and, to a lesser extent, by increased temperature [16]. The volume of the fluid also influences major and trace component activities [17]. The observation of small-scale hydrothermally altered pegmatites that contain incompatible elements could be an effective method for tracking the redistribution mechanisms of these elements.

REFERENCES

[1] Linnen R. L., M. Van Lichtervelde, P. Černý (2012) Granitic pegmatites as sources of strategic metals, Elements, **8**(4), 275–280.

[2] Ballouard C., M. Massuyeau, M. A. Elburg et al. (2020) The magmatic and magmatichydrothermal evolution of felsic igneous rocks as seen through Nb-Ta geochemical fractionation, with implications for the origins of rare-metal mineralizations, Earth Sci. Rev., **203**, 103115.

[3] Černý P., T. S. Ercit (2005) The classification of granitic pegmatites revisited, The Canad. Mineral., **43**(6), 2005–2026.

[4] Georgieva S., R. D. Vassileva, G. Milenkov (2022) Mineral association in pegmatites from the Djurkovo Pb-Zn deposit, Central Rhodopes: preliminary results. In: Proceedings of the National Conference "GEOSCIENCES 2022", Sofia, Rev. Bulg. Geol. Soc., **83**(3), 19–22.
[5] Georgieva S., R. D. Vassileva, G. Milenkov et al. (2023) Rare-earth element mineralization in altered pegmatites from the Djurkovo Pb-Zn deposit, Central Rhodopes. In: 17th SGA Biennial Meeting "Mineral Resources in a Changing World", 28th August–1st September 2023, Zurich, 31–34.
[6] Georgieva S., R. D. Vassileva, V. Grozdev et al. (2023) Redistribution of incompatible elements during hydrothermal alteration of pegmatite from the Djurkovo Pb-Zn deposit, Central Rhodopes, Review Bulg. Geol. Soc., Geosciences 2023, **84**(3), 35–38.
[7] Milenkov G., R. D. Vassileva, S. Georgieva (2022) Critical elements in allanite and titanite from pegmatites in the Petrovitsa Pb-Zn deposit, Central Rhodopes, Bulgaria. In: Christie A. B. (ed.) Proceedings of the 16th SGA Biennial Meeting, Rotorua, New Zealand, 28–31 March 2022, V 1, 255–258.
[8] Vassileva R. D., S. Georgieva, G. Milenkov (2022) Rare earth mineral association in pegmatites from Kroushev Dol Pb-Zn deposit. In: Irena Peytcheva et al. (Eds) XXII International Congress of the Carpathian-Balkan Geological Association (CBGA), Geologica Balc., Abstracts, 7–11 September 2022, p. 340.
[9] Vassileva R. D., S. Georgieva, G. Milenkov et al. (2023) Pegmatite REE-mineral association from the Kroushev Dol base metal deposit (south Bulgaria): mineral replacements and timing of formation, 17th SGA Biennial Meeting "Mineral Resources in a Changing World", 28th August – 1st September 2023, Zurich, 242–245.
[10] Vassileva R. D., S. Georgieva, J. Cempírek et al. (2023) Garnet (REE+Y)-bearing mineral association in pegmatite from the Chepino lithotectonic Unit, Western Rhodopes, Review of the Bulgarian Geological Society, Geosciences 2023, **84**(3), 63–66.
[11] Marchev P., M. Kaiser-Rohrmeier, C. Heinrich et al. (2005) Hydrothermal ore deposits related to post-orogenic extensional magmatism and core complex formation: The Rhodope Massif of Bulgaria and Greece, Ore Geol. Rev., **27**, 53–89.
[12] Buret Y., K. Kouzmanov (2011) Polymetallic mineralization in the Laki mining district Southern Bulgaria: Paragenesis and fluid evolution. In: Abstract Volume 9th Swiss Geoscience Meeting, Zurich, 11–13 November 2011, Symposium 2: Mineralogy, Petrology, Geochemistry, 88–89.
[13] Vassileva R. D., V. Grozdev, I. Peytcheva et al. (2020) Andradite from Pb-Zn Djurkovo deposit, Central Rhodopes: chemical composition and U/Pb dating, Rev. Bulg. Geol. Soc. (Geosciences 2020), **81**(3), 58–60.
[14] Buret Y., K. Kouzmanov, R. Spikings, Y. Gerdjikov (2013) Timing of polymetallic Pb-Zn mineralisation in the Laki district, southern Bulgaria – constraints from 40Ar/39Ar dates. In: Abstract Volume 11th Swiss Geoscience Meeting Lausanne, 15th – 16th November 2013, Symposium 2: Mineralogy, Petrology, Geochemistry, 49–50.
[15] Migdisov A., A. E. Williams-Jones, J. Brugger, F. A. Caporuscio (2016) Hydrothermal transport, deposition, and fractionation of the REE: Experimental data and thermodynamic calculations, Chem. Geol., **439**, 13–42.

[16] Adam J., M. Locmelis, J. C. Afonso et al. (2014) The capacity of hydrous fluids to transport and fractionate incompatible elements and metals within the Earth's mantle, Geochem. Geophys. Geosyst., **15**, 2241–2253.
[17] Wood B. J., J. D. Blundy (2002) The effect of H_2O on crystal-melt partitioning of trace elements, Geochim. Cosmochim. Acta, **66**(20), 3647–3656.

[1]*Geological Institute, Bulgarian Academy of Sciences,*
Akad. G. Bonchev St, Bl. 24, 1113 Sofia, Bulgaria
e-mails: sylvina@geology.bas.bg, rosivas@geology.bas.bg, valgrozdev@gmail.com, georgimilenkov7@gmail.com, elitsa.s@gmail.com

[2]*Department of Geological Sciences, Masaryk University, 611 37 Brno, Czech Republic*
e-mail: jan.cempirek@gmail.com, rskoda@sci.muni.cz